The response of the wall shear stress in uniformly and nonuniformly accelerating pipe flows

L.R. Joel Sundstrom

Division of Fluid and Experimental Mechanics
Luleå University of Technology
SE-971 87, Luleå, Sweden
joel.sundstrom@ltu.se

Michel J. Cervantes

Division of Fluid and Experimental Mechanics
Luleå University of Technology
SE-971 87, Luleå, Sweden
michel.cervantes@ltu.se

ABSTRACT

Wall shear stress measurements in an accelerating turbulent pipe flow have been performed. Four different imposed accelerations have been studied including one uniform and three non-uniform ones. The initial-to-final Reynolds numbers as well as the acceleration time were approximately the same for each case, thereby isolating the effect of the type of acceleration. Data have been taken using hot-film anemometry, and it has been established that the time-development for each case is qualitatively similar, although there are significant quantitative differences between each case. The previously established view that the time-development of an accelerating flow resemble a laminar-to-turbulent bypass transition is confirmed. An explanation for the transitional behavior is sought through the Poisson equation describing the pressure fluctuations. It is postulated that the fast pressure induces asymmetries in the time-development of the wall-normal velocity fluctuations thereby leading to a route to transition. Due to lack of data, however, the proposed explanation cannot be confirmed or rejected, for that, further experimental as well as numerical studies have to be performed.

Introduction

Unsteady turbulent flows are ubiquitous in engineering applications including, e.g., turbomachinery and the start up and stopping of hydropower plants. A flow quantity of particular interest is the wall shear stress, of which knowledge can provide information on the current flow domain (laminar/turbulent) or for engineering applications such as transient leak detection, and flow rate measurements. In this paper, hot-film measurements of the wall shear stress in a turbulent pipe flow subjected to uniformly and non-uniformly accelerations are presented.

Modeling of the wall shear stress in transient turbulent flows has been an ongoing research topic for more than 70 years, and it is also the ultimate goal of the present study, namely, to develop a model for transient friction to be utilized for flow rate measurements in hydropower. Two commonly utilized models approximates the wall shear stress by making it dependent on i) the instantaneous mean flow velocity, local acceleration and convective acceleration, and ii) instantaneous mean flow velocity and weights of past changes (see Bergant *et al.*, 2001). The former method is of trial and error and lacks theoretical background, whereas the latter approach is an extension of the laminar problem, first solved analytically by Zielke (1968), and later on extended and generalized by Brereton (2000).

The development of unsteady friction models is of engineering interest, but, studying the response of the turbulence in wall-bounded flows is of interest from a fundamental perspective as well because of the non-equilibrium features of the turbulence that are not present in a statistically steady flow. One of the first detailed studies of transient turbulent pipe flows was performed by Maruyama *et al.* (1976) who used electrochemical sensors to measure the distribution of the axial velocity and the wall shear stress in a flow undergoing a step-change from 5,000 to 10,000 in Reynolds number; $Re = U_b D/\nu$, with U_b, D and ν being the bulk velocity, pipe diameter and kinematic viscosity, respectively. They found that new turbulence was generated next to the wall, and that this newly generated turbulence gradually propagated toward the pipe axis.

Using laser Doppler velocimetry (LDV), He & Jackson (2000) measured all three components of the ensemble-averaged mean and turbulent fluctuating velocities in a pipe flow undergoing a close-to-uniform acceleration in the Reynolds number range 7,000-42,000. Like Maruyama *et al.* (1976), they found that the turbulence responds close to the wall, and furthermore, that only the streamwise component responds initially. Subsequently, the two other components of the turbulent velocities increase, and do so simultaneously over a significant portion of the pipe radius, owing to increased pressure-strain. Away from the wall ($y^+ > 50$, say), all three components display similar developments.

Greenblatt & Moss (2004) investigated the response of the mean and turbulent axial velocities using LDV in a turbulent pipe flow accelerating rapidly between $Re_0 = 31,000$ and $Re_1 = 81,000$. In addition to the aforementioned generation of turbulence in the vicinity of the wall, they found that turbulence, albeit after an initial delay, was generated also at $y^+ = 300$. This additional generation of turbulence was not observed by Maruyama *et al.* (1976) nor He & Jackson (2000). The authors postulated that the larger Reynolds numbers involved in their study could serve as an explanation for the additional generation of turbulence. Such argument is supported by the fact that u'_{rms}, for steady state flows as the Reynolds number is increased, does develop a second peak at a large wall-normal distance (see Hultmark *et al.*, 2010).

He *et al.* (2011) used flush-mounted hot-film anemometry to measure the wall shear stress in an accelerating pipe flow covering initial-to-final Reynolds numbers in the range 4,500-210,000. They found that the time-development of the wall shear stress was characterized by three distinct phases; initially during the first phase, inertial effects dominated the response and the wall shear stress could be accurately predicted using a laminar formulation. For small times, the increase of τ was faster than a corresponding quasi-steady flow, but as time proceeded, the delayed response of the turbulence made τ undershoot the corresponding steady value. Subsequently, during the second phase, there was a rapid generation of new turbulence and τ increased very rapidly, in some cases again overshooting the quasi steady value. Finally, the last phase was characterized by an asymptotic convergence of τ toward the value prevailing at the final Reynolds number.

Albeit the aforementioned experimental studies have provided significant understanding of transient flows, detailed information about the generation, redistribution and propagation of the turbulence has not been extracted from these studies owing to the experimental difficulties involved in performing such analyses. Recently,

S. He, M. Seddighi and co-workers have performed a series of direct numerical simulations (DNS) of impulsively and uniformly accelerating turbulent flows (He & Seddighi, 2013; Seddighi *et al.*, 2014; He & Seddighi, 2015). The detailed information made available through the DNSs have shown that the transient period between the two turbulent states closely resembles the spatial development of a flat plate laminar-to-turbulent bypass transition. In particular, the three-stage response of the wall shear stress found by He *et al.* (2011) are analogous to the three spatial regions discussed in the bypass transition; namely, the pre-transitional, transitional and fully turbulent regions.

Although DNSs have increased the understanding of transient flows, there still remain questions to be answered; in particular, the transitional phase has been shown to coincide with the generation of new turbulence structures but the cause of the transition has not been elucidated. Furthermore, turbulent flows undergoing a non-uniform acceleration has received less attention than uniformly/impulsively accelerating flows, even though many flows encountered in engineering applications are subjected to non-uniform accelerations. Since the response following either a step-change or a uniform acceleration are qualitatively similar, although the former represents a more severe case, it can be expected that the time-development of the turbulence following a non-uniform acceleration should also exhibit the transitional behavior.

The purpose of the present paper is twofold; i) to verify that a non-uniformly accelerating flow exhibit transitional behavior, and ii) to discuss potential routes leading to the transition. To that end, as fore mentioned, hot-film anemometry measurements in uniformly and three non-uniformly accelerating pipe flows have been performed. The range of Reynolds numbers was held fixed, $Re_0 = 11,500$ and $Re_1 = 35,500$, thus, the influence of different flow rate histories could be isolated.

Experimental apparatus and test conditions

Measurements were taken in a 10.4 m straight pipe of internal diameter $D = 100$ mm. The working fluid, water kept at $20^{\circ}C$ $\pm 0.1^{\circ}C$, was supplied to the test section through a tubing system utilizing an Oberdorfer N1100 gear pump. The pump provided highly repeatable flow rate histories among different repetitions of nominally similar runs. The flow rate was monitored using a Krohne OPTIFLUX electromagnetic flow meter with an accuracy at steady operating conditions of $\pm 0.7\%$.

Wall shear stress measurements were carried out for a turbulent flow ramping between $Re_0 = 11,500$ to $Re_1 = 35,500$ over $\Delta t \approx 7.5$ s for four different bulk flow accelerations. The flow rate histories were constructed to produce accelerations like (i) a slow initial acceleration followed by a more rapid bulk flow change, (ii) a fast initial acceleration followed by a slower acceleration, (iii) a flow rate history with an inflection point, and (iv) a constant acceleration, see figure 1 for the Reynolds number histories. For each case, the measurements were repeated approximately 300 times, with each realization being initiated from statistically independent states.

Wall shear stress measurements

Wall shear measurements were performed $L = 80D$ downstream the test section inlet at one circumferential position using a 55R46 hot-film sensor from Dantec Dynamics. Whether or not it is an issue that measurements were performed at a single circumferential position is a moot question; for, the wall shear stress measurements performed by He *et al.* (2011) in an accelerating pipe flow did exhibit significant spatial dependence in one out of eight cases investigated. Their measurement stations were located at $L = 48D$ and $L = 52D$ from the inlet, and each section was equipped with three evenly spaced hot-film sensors. Negligible spatial dependence

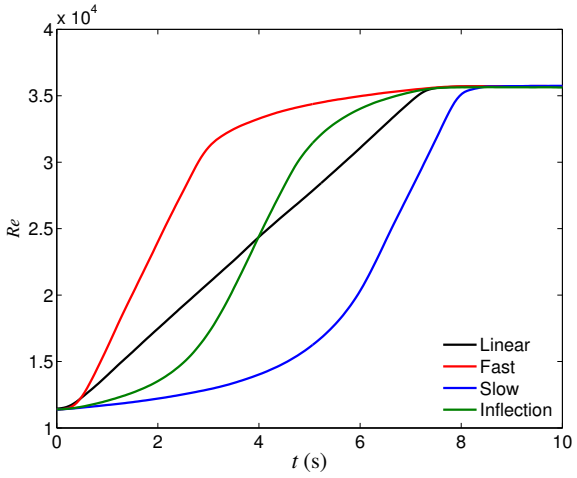

Figure 1: Reynolds number histories for the investigated cases.

was found for mildly accelerating flows ($\delta < 0.09$) based on the similarity variable $\delta = \nu/u_{\tau 0}^2 (1/U_{b0})(\mathrm{d}U_b/\mathrm{d}t)$. The friction velocity is denoted by u_τ, subscripts '0' refer to the initial values. For $\delta = 0.9$, however, non-negligible axial and circumferential dependencies were found. The cause of the asymmetries is not clear but the present authors have observed similar asymmetries in yet unpublished work for $\delta = 0.013$. A large value of δ does not, however, seem sufficient to trigger asymmetries, for, in the present experimental apparatus, measurements have been taken with $\delta = 0.026$ at eight evenly distributed circumferential locations, and at two axial locations separated by $L = 10D$ with differences falling within the experimental accuracy. By defining δ for the present nonlinearly accelerating flows based on the maximum acceleration rate, all investigated cases fall within $\delta < 0.013$. This is a factor two smaller than the aforementioned thoroughly investigated case, but, almost equal to the case in which asymmetries were found. Therefore, it cannot be excluded that the results presented herein are spatially independent.

The hot-film sensor was operated at an overheat ratio of 8%, controlled using a Dantec Streamline Pro Constant Temperature Anemometry system. The sensing element of the probe is 0.20 mm $\times$ 0.75 mm in the streamwise and circumferential directions, respectively. The maximum dimensions of the sensor in viscous units corresponded to $4\delta_\nu \times 15\delta_\nu$, where $\delta_\nu = \nu/u_{\tau 1}$ is the steady-state viscous length scale at $Re_1 = 35,500$. Thus, spatial averaging should not influence the results because the sensing element was smaller than $20\delta_\nu$ (see Blackwelder & Haritonidis, 1983).

Calibration of the sensor was performed *in situ* twice a day. The hot-film voltage and the flow rate were recorded for 180 s (preceded by a 45 s stabilization time to ensure steady conditions) at six Reynolds numbers in the range $5,000 < Re < 70,000$. In steady state, τ can be directly related to the pressure drop $\tau = \Delta p(D/4L)$. In the present setup, however, such approach for estimating the wall shear stress was not appropriate because small pressure drops were encountered (the minimum of $\mathrm{d}p/\mathrm{d}x$ was $0.5\,\mathrm{Pa\,m^{-1}}$) which could not be measured with sufficient accuracy. Instead, estimates of the wall shear stresses were obtained from $\tau = (\rho U_b^2 f)/8$, where f is the friction factor, and ρ the fluid's density. The friction factor was extracted from Prandtl's friction law for smooth pipes (see Pope, 2000). The estimated values of the wall shear stresses were aptly fitted to the measured hot-film voltages, E, by

$$\tau^{1/3} = A + BE^2. \qquad (1)$$

The fluctuations in the hot-film voltage have been accounted for as described in Goldstein (1996); A and B are calibration constants. The hot-film signal was acquired using a PXI system consisting of a 24-bit (NI-4472) card at a rate of 1 kHz.

Although each case was repeated approximately 300 times, scatter was ubiquitous in the data because the wall shear stress is a highly fluctuating quantity ($\tau'/\tau \sim 0.4$ in steady flow). To reduce the scatter, ensemble averages of the mean and the root mean square (r.m.s.) turbulent fluctuations were calculated using the window-averaging method introduced by He & Jackson (2000)

$$\begin{aligned} \tau_k &= \frac{1}{NM}\sum_{i=1}^{N}\sum_{j=1}^{M}\tau_{i,j+(k-1)M}, \qquad k=1,2,3,...,L \\ \tau'_k &= \left[\frac{1}{NM}\sum_{i=1}^{N}\sum_{j=1}^{M}(\tau_{i,j+(k-1)M}-\tau_k)^2\right]^{1/2} \quad k=1,2,3,...,L. \end{aligned} \tag{2}$$

Where τ_k and τ'_k are the mean and the turbulent components of the wall shear stress in the kth window, respectively. In (2), L is the number of windows into which the data are divided, M is the number of samples in each window, and N is the number of repeated runs. M was chosen as 50, a value that reduced the scatter but did not introduce gradients of the calculated quantities in the windows. In the remainder of the paper, the convention in (2), with the index dropped, will be used. In He & Seddighi (2013), it was shown that it is instructive to consider the perturbation from the initial value prevailing before an acceleration is imposed, i.e. $\tau^{\wedge}(t) = \tau(t) - \tau(0)$ instead of the response of $\tau(t)$. Therefore, the results will be presented in terms of $\tau^{\wedge}$ (and $\tau'^{\wedge}$).

EXPERIMENTAL UNCERTAINTIES

Two principal sources of error in the present setup derived from (i) uncertainties in the sensor calibration and drifting of the hot-film voltage due to sensor contamination, and (ii) insufficient number of repeated runs.

Effort was spent to minimize the errors by (i) installing a water filter that collected particles larger than five microns, updating the calibration curve twice a day and by using a cooling system that kept the water temperature constant within $20 \pm 0.1°C$, and (ii) by repeating each measurement approximately 300 times and by using the previously described window-averaging.

The main errors in the calibration curve are related to (i) the accuracy of the estimated value of τ and (ii) the uncertainties in the hot-film voltage. Uncertainties in τ mainly derives from inaccuracies in the friction factor, the flow rate and the pipe diameter. From analyses of large sets of data, the random error of τ was estimated between $\pm 0.3\%$ and $\pm 0.8\%$, with larger uncertainties at lower Reynolds numbers. The systematic error was estimated to be $\pm 2\%$. The main errors in the hot-film voltage arose from drifting of the water temperature, sensor contamination and the sampling time at each calibration point. The random and systematic errors of the hot-film voltage were estimated to be $\pm 0.2\%$ and $\pm$ 1%, respectively. By combining these uncertainties, the total uncertainty of the values used from the calibration curve at a 95% confidence level was estimated to be $\pm 8\%$. The large uncertainty in τ compared to the numbers presented above arises because $\tau \sim E^6$.

The errors resulting from the finite number of repeated runs are subtle to estimate. The accumulated mean value in each window was investigated as well as the fluctuations between neighboring windows. Uncertainties due to fluctuations between windows were estimated to ± 2 %, whereas the uncertainties due to the convergence of the mean value was estimated to $\pm$ 3%. Taken together, the total uncertainty in the values of τ presented below is thus of order $\pm\sqrt{8^2+2^2+3^2} \approx \pm 9\%$.

RESULTS

The results section starts with a general discussion about the response of $\tau^{\wedge}$. A more detailed discussion is subsequently presented by analyzing the response of the r.m.s. turbulent wall shear stress. To aid the upcoming discussion, the equation governing the ensemble-averaged mean perturbation velocity, $U^{\wedge}$, is presented

$$\frac{\partial U^{\wedge}}{\partial t} = -\frac{1}{\rho}\frac{\mathrm{d}p^{\wedge}}{\mathrm{d}x} + \frac{1}{r}\frac{\partial}{\partial r}\left[r\left(\nu\frac{\partial U^{\wedge}}{\partial r} - \overline{u'v'}^{\wedge}\right)\right], \tag{3}$$

in which circumferential and axial independence (despite the previous discussion) have been assumed.

Figure 2 shows the time-developments of the ensemble-averaged perturbation wall shear stresses from the four cases. The response of $\tau^{\wedge}$ following a near-uniform acceleration display the aforementioned three-stage response; initially, during stage one $t < 3.4$ s, the ensemble averaged flow field is mainly governed by inertial effects, and consequently, $\tau^{\wedge}$ is accurately described by a laminar formulae (included as a dash-dotted line). To the leading order, the formula for $\tau^{\wedge}$ for a laminar flow accelerating linearly over a duration $\Delta t = t_1$ s is

$$\tau^{\wedge} = 2\rho\frac{\mathrm{d}U_b}{\mathrm{d}t}\sqrt{\frac{\nu}{\pi}}\left[\sqrt{t} - \mathrm{H}(t-t_1)\sqrt{t-t_1}\right], \tag{4}$$

where H(·) is the Heaviside step function. A slightly different version of (4) was derived by He & Ariyaratne (2011), and verified against experimental data in He *et al.* (2011). Although not explicitly presented, (4) can be derived from the analysis presented in Brereton (2000). In here, the acceleration is not exactly linear, particularly during the early stages, since the pump could not provide such flow rate history. Therefore, there is disagreement between the analytical solution and the present measurement initially. Following the close-to-laminar initial response, stage two is initiated and $\tau^{\wedge}$ increases more rapidly than the corresponding laminar flow for 3.4 s $< t <$ 7 s. Subsequently, during the third stage for $t >$ 7 s, the wall shear stress approaches the value dictated by the final Reynolds number. For the cases of nonlinearly accelerating flows, the time-developments of the wall shear stresses are qualitatively similar to that of the linear case, thus indicating that the same mechanisms underlies the flow response. The time histories of the flow rate can, however, be traced in the details of the responses of the wall shear stresses. Specifically, for a fast initial acceleration, $\tau^{\wedge}$ increases more rapidly than for any other case, whereas for a slow initial acceleration, there is a very slow initial variation of $\tau^{\wedge}$. The response of $\tau^{\wedge}$ for the inflection point type of bulk flow acceleration, as expected, falls in between those of the fast and the slow accelerations.

An interesting characteristic that $\tau^{\wedge}$ exhibits for the case of a fast initial acceleration is that the wall shear stress remains approximately constant for 2.9 s $< t <$ 3.3 s. From (4) and also illustrated by the dash-dotted line in figure 2 (a) it is clear that the wall shear stress in a laminar flow decreases when $\mathrm{d}U_b/\mathrm{d}t$ vanishes. Although no explicit, simple formula like (4) can be derived for a nonlinearly accelerating laminar flow, $\tau^{\wedge}$ still decreases when the inertia force is suddenly decreased (but not necessarily completely relaxed) for such case. From figure 1 it is seen that $\mathrm{d}U_b/\mathrm{d}t$ decreases appreciable around $t = 3$ s. The present flow is turbulent, and the time-development of $\tau^{\wedge}$ cannot be explained by laminar arguments alone. However, owing to the linearity of (2), the response

of $U^\wedge$ can be split into a (laminar) contribution resulting from the applied pressure gradient and a turbulent contribution resulting from the forcing $\overline{u'v'}^\wedge$. From figure 2 (b), it is clear that $\tau'^\wedge$, and consequently also $\overline{u'v'}^\wedge$, increases rapidly around $t = 2.9$ s. Thus, the laminar contribution to $\tau^\wedge$ decreases whereas the turbulent contribution increases, the net effect being that the two contributions counteracts each other thereby resulting in an approximately constant wall shear stress. This feature is similar to what is observed in pulsating turbulent flows for a range of forcing frequencies, ω, and time-averaged Reynolds numbers; namely, that the phase-averaged wall shear stress remain approximately constant over a period of the flow cycle. Similarly as observed inhere, the laminar and turbulent portions of the flow counteracts each other thus resulting in the approximately constant wall shear stress (see, e.g., figure 2b in Scotti & Piomelli, 2002). In a pulsating flow, this cancellation is manifested by a peculiar result; namely, an amplitude of the phase-averaged wall shear stress that is smaller in a turbulent flow compared to a laminar flow subjected to the same time-averaged Reynolds number and forcing frequency (for a further discusson, see Scotti & Piomelli, 2001; Sundstrom *et al.*, 2016).

With the main features of the time-developments of $\tau^\wedge$ established, the details underlying the responses are now discussed. This is most effectively done by considering the r.m.s. turbulent (perturbation) wall shear stress which, through a Taylor series expansion, can be related to the near-wall ($y^+ < 2$, say; the increased curvature of the near-wall velocity profile makes the linear approximation more restrictive compared to a steady flow) streamwise r.m.s. velocity $u'^\wedge \approx (\tau'^\wedge/\mu)y$. Following the commencement of the flow rate excursion, the near-wall velocity gradient increases, which in turn, causes an increase of $u'^\wedge$ through increased turbulence production. The increased turbulence production is, however, not associated with the generation of new turbulent structures; rather, Seddighi *et al.* (2014) have shown that the energy growth is associated with elongation/amplification of the near-wall streaks that preexisted before the commencement of the acceleration. Since there is hardly any generation of new turbulence structures during this initial phase, the correlation between u' and v' grows much slower than in a steady flow at the same instantaneous Reynolds number. Consequently, the perturbation Reynolds shear stress, $\overline{u'v'}^\wedge$, is much smaller than the inertia effect thus allowing this term to be neglected from (3), thereby justifying the laminar formula of $\tau^\wedge$ during the initial phase of the acceleration.

The initial, relatively slow growth of $\tau'^\wedge$ is readily explained by the amplification of the near wall streaks. At certain points in time, however, new turbulence structures are generated which is manifested by a faster growth of $\tau'^\wedge$. The cause of this turbulence generation has not been established in previous studies but the present data do exhibit certain characteristics that can aid the understanding of the second phase of the transition. Specifically, in figure 2 (b), the horizontal line marks the approximate start of the second phase. It seems that the more rapid growth of $\tau'^\wedge$ correlates with a threshold value of $\tau'^\wedge$, since the initiation of the second phase, within experimental errors, coincides with the crossing of the threshold value. An interpretation of this correlation could then, from an ensemble-averaged view, be that the elongated near-wall streaks starts to break down when the disturbances reach a threshold level. Whereas the increased growth rate of the near-wall turbulence correlates with an absolute level of $\tau'^\wedge$, the absolute value of $\tau^\wedge$ at the onset of the transitional phase is not equal among the cases. However, instead of considering the instantaneous value of $\tau^\wedge$ it is instructive to define the accumulated wall shear stress

$$\hat{\tau} = \int_0^t \tau^\wedge(t')\mathrm{d}t', \tag{5}$$

since this quantity is related to the accumulated near-wall turbulence production, i.e., the perturbation energy. Figure 2 (c) shows the accumulated wall shear stress, the horizontal line included in the figure marks the value of $\hat{\tau}$ at the onset of the transitional phase for the case of a fast initial acceleration. Comparing figure 2 (b) and (c), it is seen that the accumulated wall shear stress in each case is approximately equal at the onset of transition, thus suggesting that the generation of new turbulence structures correlates with $\hat{\tau}$. The streamwise perturbation velocity fluctuations and the perturbation Reynolds shear stress increase through production

$$P_{\overline{u'u'}^\wedge} = \overline{u'v'}_0 \frac{\partial U^\wedge}{\partial y} + \overline{u'v'}^\wedge \frac{\partial U_0}{\partial y} + \overline{u'v'}^\wedge \frac{\partial U^\wedge}{\partial y}, \tag{6a}$$

$$P_{\overline{u'v'}^\wedge} = \overline{v'v'}_0 \frac{\partial U^\wedge}{\partial y} + \overline{v'v'}^\wedge \frac{\partial U_0}{\partial y} + \overline{v'v'}^\wedge \frac{\partial U^\wedge}{\partial y}. \tag{6b}$$

The DNS by Seddighi *et al.* (2014) have shown that $\overline{v'v'}^\wedge$ remain largely unchanged initially following the commencement of an acceleration, thus implying that only the first term in (6b) contribute to the production of $\overline{u'v'}^\wedge$. Using this and integrating (6) with respect to time very close to the wall reveals the connection between the accumulated wall shear stress and $\tau'^\wedge$. This argument does not, however, explain why the flow transitions when a threshold of $\hat{\tau}$ and/or $\tau'^\wedge$ is reached; rather, the mechanism that generates excess Reynolds shear stress must be found since, without a rapid generation of $\overline{u'v'}^\wedge$, the flow would remain quasi-laminar indefinitely. From (6), a generation of $\overline{v'v'}^\wedge$ implies a more rapid increase of the Reynolds shear stress. Since $\overline{v'v'}$ extracts energy through pressure-strain; $\phi_{22} = \overline{2p'\partial v'/\partial r}$, a possible explanation for the transition could be through increased pressure fluctuations. The fluctuating pressure can be both directly and indirectly coupled to the ensemble-averaged velocity gradient since p' satisfies the following Poisson equation

$$\frac{1}{\rho}\nabla^2 p' = -2\frac{\partial U}{\partial r}\frac{\partial v'}{\partial x} + (\boldsymbol{\omega}'\cdot\boldsymbol{\omega}' - \overline{\boldsymbol{\omega}'\cdot\boldsymbol{\omega}'}) - \left[\nabla\mathbf{u}' : \nabla\mathbf{u}' - \overline{\nabla\mathbf{u}' : \nabla\mathbf{u}'}\right], \tag{7}$$

where $\boldsymbol{\omega}'$ is the vorticity fluctuations, and the double-dots denotes a doubly contracted product. The indirect coupling to the ensemble-averaged velocity gradient is through the transport equation for the ensemble-averaged enstrophy $\overline{\boldsymbol{\omega}'\cdot\boldsymbol{\omega}'}$ (see Tennekes & Lumley, 1972). The fluctuating pressure can be split into a fast contribution satisfying (7) with only the first term on the right hand side, a slow contribution satisfying (7) with the two terms within parentheses, and a homogeneous pressure satisfying the boundary conditions. Following the commencement of an acceleration it has been established that $\tau^\wedge$ increases, and so too does $\partial U/\partial r$ away from the wall as time elapses and the excess shear generated at the wall diffuses into the flow. Thence, it is expected that the rapid pressure fluctuations increase as time elapses following the onset of an acceleration. Such increase of the rapid (wall) pressure fluctuations has indeed been measured by the present authors in yet unpublished work (not presented in here). The increase is, however, not monotonic; rather, the fluctuating pressure oscillates following the commencement of an acceleration. At the points in time when the oscillations peak, there is potential for an increase in $\overline{v'v'}$. Now, it is postulated that the excess pressure fluctuations correlates with $\partial v'/\partial r$ only at certain circumferential positions, thus implying that $\overline{v'v'}$ increases only at those positions. Such argument is supported by the results presented in He *et al.* (2011); for, they reported large circumferential

asymmetries in the response of the wall shear stress when the imposed acceleration was strong. From (1) and (6), the asymmetry should ultimately stem from asymmetries in the ensemble-averaged wall-normal velocity fluctuations. Now, such asymmetries may exist even for lower acceleration rates, but less pronounced compared to what was reported in He *et al.* (2011). Thence, if the fast pressure initiate asymmetries, this would in turn induce vorticity fluctuations. As the vorticity fluctuations become stronger, the slow pressure fluctuations would increase more rapidly and this could then lead to the transition and the very rapid increase of $\tau'^{\wedge}$. Clearly, wall shear stress data alone cannot justify the reasoning just presented. For that, direct numerical simulations allowing the required derivatives to be calculated are needed.

CONCLUSIONS

The time-development of the wall shear stress in a turbulent pipe flow following a close-to-uniform and three nonlinear accelerations have been investigated using hot-film anemometry. Previous studies of turbulent flows undergoing either a step change or a linear change in the flow rate have shown that the time-development between the initial and final states resembles a laminar-to-turbulent bypass transition, exhibiting pre-transitional, transitional and fully turbulent states. During the initial phase of the pre-transition, only the streamwise velocity fluctuations increase whereas the wall-normal and circumferential (spanwise for channel flow) components remain unchanged. As a consequence, much of the flow characteristics can be described using laminar formulations. The data presented herein show similar transitional time-development also for non-uniform accelerations, and for the uniform acceleration, good agreement with an analytical expression for the wall shear stress is found. Albeit each case show transitional behavior, the details of the time-developments of the wall shear stresses are dependent on the particular flow rate change.

When the initial acceleration is fast, the time-development of the wall shear stress displays a feature that is similar to what has been found for pulsating flows. The particular feature is that the wall shear stress remain approximately constant for a period of time. For a pulsating flow, this is manifested in that the amplitude of the oscillating wall shear stress is smaller in a turbulent flow than a corresponding laminar one for certain time-averaged Reynolds numbers and forcing frequencies. The phenomenon is related to a phase shift between the response of the turbulence and the imposed pressure gradient.

An explanation for the observed transitional behaviour is sought through the (Poisson) equation for the pressure fluctuations. It is postulated that the fast pressure, which responds immediately following an acceleration due to the generated shear, develop asymmetries in the wall-normal velocity fluctuations. These asymmetries subsequently lead to large vorticity fluctuations that will activate the slow pressure. The excess (slow) pressure fluctuations thus induced would lead to an increase in the wall-normal velocity fluctuations and corresponding departures from the laminar-like behavior during the late stage of pre-transition. As the pressure fluctuations and the wall-normal fluctuations increase in tandem, this lead to a more rapid increase of $\overline{v'v'}$, which ultimately initiates the transition. Wall shear stress measurements alone cannot confirm, nor reject the postulated route to transition. For that, direct numerical simulations are needed in order to solve the Poisson equation for the pressure fluctuations.

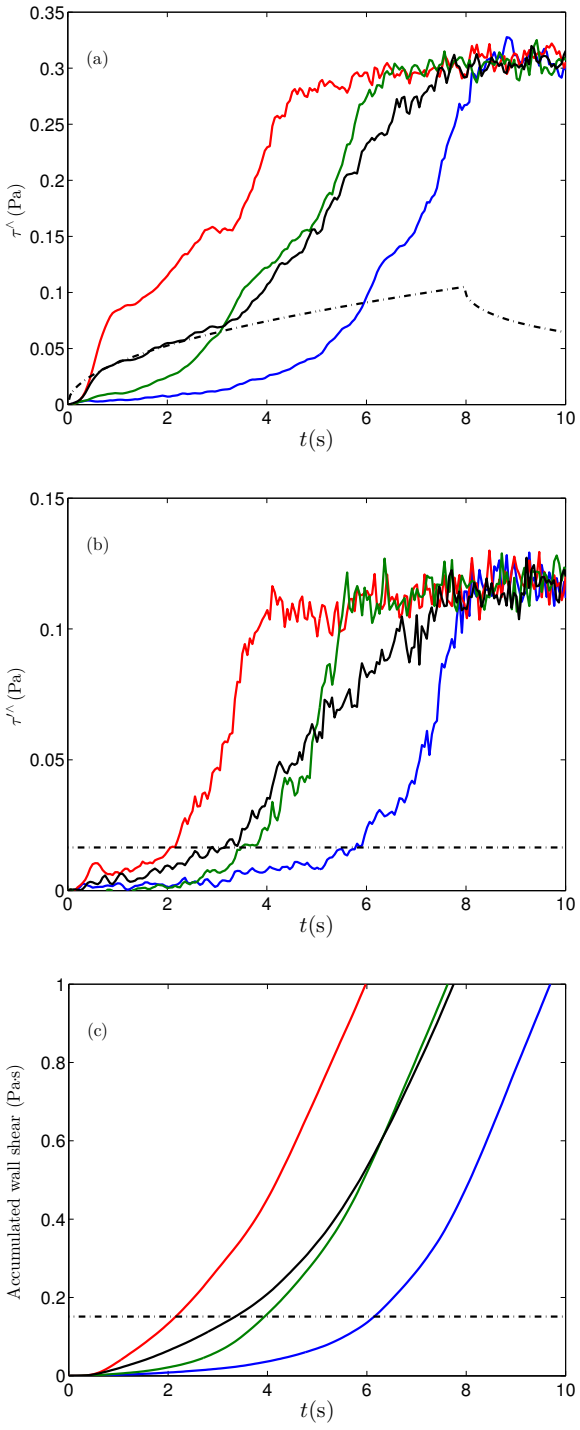

Figure 2: Time-developments of a) $\tau^{\wedge}$, b) $\tau'^{\wedge}$ and c) $\hat{\tau}$. For caption, see figure 1.

REFERENCES

Bergant, A., Simpson, A.R. & Vitkovsky, J. 2001 Developments in unsteady pipe flow friction modelling. *Journal of Hydraulic Research* **39** (3), 249–257.

Blackwelder, R. F. & Haritonidis, J. H. 1983 Scaling of the bursting frequency in turbulent boundary layers. *J. Fluid Mech.* **132**, 87–103.

Brereton, G. J. 2000 The interdependence of friction, pressure gradient, and flow rate in unsteady laminar parallel flows. *Physics of Fluids* **12** (3), 518.

Goldstein, R.J. 1996 *Fluid mechanics measurements*, 2nd edn. Taylor& Francis.

Greenblatt, D. & Moss, E.A. 2004 Rapid temporal acceleration of a turbulent pipe flow. *J. Fluid Mech.* **514**, 65–75.

He, S. & Ariyaratne, C. 2011 Wall shear stress in the early stage of

unsteady turbulent pipe flow. *J. Hydraul. Engng.* **137**, 606–610.
He, S., Ariyaratne, C. & Vardy, A.E. 2011 Wall shear stress in accelerating turbulent pipe flow. *J. Fluid Mech.* **685**, 440–460.
He, S. & Jackson, J.D. 2000 A study of turbulence under conditions of transient flow in a pipe. *J. Fluid Mech.* **408**, 1–38.
He, S. & Seddighi, M. 2013 Turbulence in transient channel flow. *J. Fluid Mech.* **715**, 60–102.
He, S. & Seddighi, M. 2015 Transition of transient channel flow after a change in Reynolds number. *J. Fluid Mech.* **764**, 395–427.
Hultmark, M., Bailey, S.C.C. & Smits, A.J. 2010 Scaling of near-wall turbulence in pipe flow. *J. Fluid Mech.* **649**, 103.
Maruyama, T., T.Kuribayashi & Mizushina, T. 1976 The strutcure of the turbulence in transient pipe flows. *Journal of Chemical Engineering of Japan* **9** (6), 431–439.
Pope, S.B. 2000 *Turbulent flows*. Cambridge University Press.
Scotti, A. & Piomelli, U. 2001 Numerical simulation of pulsating turbulent channel flow. *Phys. Fluids* **13**, 1367–1384.
Scotti, A. & Piomelli, U. 2002 Turbulence models in pulsating flows. *AIAA Journal* **40** (3), 537–544.
Seddighi, M., He, S., Vardy, A. & Orlandi, P. 2014 Direct numerical simulation of an accelerating channel flow. *Flow Turbul. Combust.* **92**, 473–502.
Sundstrom, L.R.J., Mulu, B.G. & Cervantes, M.J. 2016 Wall friction and velocity measurements in a double-frequency pulsating turbulent flow. *J. Fluid Mech.* **788**, 521–548.
Tennekes, H. & Lumley, J.L. 1972 *A first course in Turbulence*, 1st edn. MIT Press.
Zielke, W. 1968 Frequency-dependent friction in transient pipe flow. *J. Basic Engineering* **90**, 109–115.